The effect of Al substitution on charge ordered $Pr_{0.5}Ca_{0.5}MnO_3$: structure, magnetism and transport

2004 J. Phys.: Condens. Matter 16 8335

(http://iopscience.iop.org/0953-8984/16/46/019)

INSTITUTE OF PHYSICS PUBLISHING JOURNAL OF PHYSICS: CONDENSED MATTER

J. Phys.: Condens. Matter **16** (2004) 8335–8344 PII: S0953-8984(04)84775-1

The effect of Al substitution on charge ordered $Pr_{0.5}Ca_{0.5}MnO_3$: structure, magnetism and transport

Sunil Nair and A Banerjee

Inter University Consortium for DAE Facilities, University Campus, Khandwa Road, Indore, 452 017, India

Received 5 August 2004, in final form 14 October 2004
Published 5 November 2004
Online at stacks.iop.org/JPhysCM/16/8335
doi:10.1088/0953-8984/16/46/019

Abstract

We report on the effect of Mn site substitution of Al on the structural, magnetic and transport properties of charge ordered $Pr_{0.5}Ca_{0.5}MnO_3$. This substitution introduces non-magnetic impurities in the Mn–O–Mn network, causes the Mn^{3+}/Mn^{4+} ratio to deviate away from unity and is seen to predominantly replace Mn^{4+} without introducing any appreciable change in the structure. The strength of charge ordering is suppressed with increasing Al doping, as is seen from AC susceptibility, the magnetocaloric effect and DC resistivity. The observation of traces of charge ordering over an extended range of impurity doping of 10%, besides being indicative of the robust nature of charge ordering in $Pr_{0.5}Ca_{0.5}MnO_3$, also underscores the relatively insignificant effect that Al substitution has on the lattice distortions and the importance of non-magnetic substitutions. For all the samples, the conductivity in the temperature range above the charge ordering transition is observed to be due to the adiabatic hopping of small polarons, whereas below the charge ordering transition, Mott's variable range hopping mechanism is seen to be valid.

1. Introduction

Manganese site doping in half-doped charge ordered (CO) manganites has emerged as a popular means of understanding the CO transition, tailoring its strength, and inducing various interesting phases in this class of materials [1–3]. Doping in the Mn site, besides introducing random impurities in the electrically and magnetically active Mn–O–Mn network, causes the Mn^{3+}/Mn^{4+} ratio to deviate away from unity, hence destabilizing the CO phase. The physical properties induced as a function of impurity substitution in these half-doped charge ordered systems are known to depend on both the electronic configuration of the impurity used as well as the bandwidth (W) of the parent composition. For example, in some cases where the dopants have partially filled d bands, doping is known to broaden the bandwidth, thus causing the ground state of some systems to change from an antiferromagnetic (AFM) insulator to a

ferromagnetic (FM) metallic one [4]. On the other hand, impurities with fully filled (or empty) d bands would dilute the Mn–O–Mn network without introducing any magnetic interactions of their own. However, in these cases, ionic size mismatch can lead to structural distortions accompanied by changes in the Mn–O bond lengths and Mn–O–Mn bond angles. Thus apart from diluting the Mn–O–Mn network, such substitutions with ionic size mismatch lead to changes in the magnetic ground states [5, 6]. The effect of Mn site substitution is seen to be drastic in the relatively narrow bandwidth systems which exhibit a CE type of spin ordering. This is indicated by the fact that in large bandwidth systems with a ferromagnetic or a layered (A type) antiferromagnetic order, long range ordering persists even up to $\geqslant$10% of impurity substitution. However, in narrow bandwidth systems with CE type of spin ordering, the CO is seen to become short-ranged with even a small amount of impurities [5]. The prediction as well as experimental verification of microscopic and mesoscopic phase separation (PS) [7, 8] has also added to considerable interest in these compounds. There are calculations [9] which show that $\leqslant$50% of hole doping makes these systems unstable towards PS into metallic FM and insulating CO phases, making the studies of systems around half-doping particularly relevant.

Here we report on the structural, magnetic and transport properties of Al doping in the Mn site of half-doped $Pr_{0.5}Ca_{0.5}MnO_3$, concentrating on the region around the CO temperature. The parent $Pr_{0.5}Ca_{0.5}MnO_3$ is known to be a prototype narrow bandwidth system, with Mn–O–Mn bond angle of about 158°. As is well known, this reduced Mn–O–Mn bond angle arises as a consequence of the co-operative rotation of the MnO_6 octahedra, and this compound is known to crystallize in an orthorhombic symmetry [10]. The low temperature ground state is known to be orbitally ordered, where the e_g orbitals hybridize with the oxygen p orbitals and participate in a co-operative Jahn–Teller distortion of the MnO_6 octahedron, thus leading to an orbital ordering of the e_g electrons in the *ab* plane accompanied by charge ordering (CO) wherein carriers localize on the manganese sites. Interestingly, recent high resolution scattering investigations indicate that long range orbital order is never achieved, and point towards the formation of an orbital domain state [11, 12]. Besides charge and orbital ordering, the spin structure is known to adopt a configuration of the CE type [13], where the (charge and orbitally ordered) Mn^{3+} and Mn^{4+} ions form ferromagnetic zig-zag chains that are coupled antiferromagnetically.

Aluminium as a dopant is particularly attractive, as is clearly seen in figure 1, which shows the ionic radii and the number of electrons in the d shell of all the Mn site dopants reported to date. Its ionic radii matches very well [14] with that of Mn^{4+}, and hence one would expect a preferential replacement of Mn^{4+} with increasing Al doping. This would also cause very little lattice distortion, an aspect which is very important considering the influence of the lattice distortions on the magnetism and transport in this class of materials. Also, the fact that Al with an empty d band is non-magnetic would ensure that unlike popular dopants like Cr [15] and Fe [16], which are known to drive the system towards a ferromagnetic ground state, Al doping would result in a more systematic reduction in the strength of the magnetic interactions driving the CO transition without adding any magnetic interaction. Though initial reports of diamagnetic Al substitution in the Mn site of half-doped manganites have indicated a suppression of both the charge ordering and the antiferromagnetic transition temperature [17, 18] and the presence of a pseudo CE phase (as is expected for systems which deviate from the ideal Mn^{3+}/Mn^{4+} (1:1) ratio), a systematic investigation of the nature and extent of this CO suppression and a quantitative analysis of the nature of conduction on either side of the (weakened) CO transition is lacking in the literature.

2. Sample preparation and characterization

Polycrystalline samples of the series $Pr_{0.5}Ca_{0.5}Mn_{1-x}Al_xO_3$ with $0 \leqslant x \leqslant 10\%$ have been prepared by the standard solid state ceramic route with starting materials Pr_6O_{11}, $CaCO_3$,

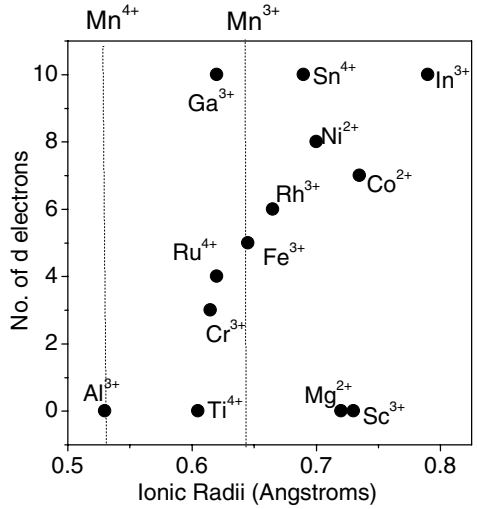

Figure 1. The number of electrons in the d shell plotted as a function of the ionic radii for all the Mn site dopants reported to date. The dashed lines correspond to the ionic radii of Mn^{3+} and Mn^{4+} ions.

MnO_2 and Al_2O_3 of at least 99.99% purity. The powdered samples were sintered at 950 °C twice for 24 h each. After regrinding, the samples were pelletized and treated at 1250 °C for 36 h and at 1350 °C for 50 h, with intermediate grindings. The x-ray diffraction (XRD) measurements were done using a Rigaku Rotaflex RTC 300RC powder diffractometer with Cu Kα radiation. All the samples were seen to be single phase, and the XRD patterns were analysed by Rietveld profile refinement, using the profile refinement package by Young *et al* [19]. Iodometric redox titrations using sodium thiosulphate and potassium iodide were performed to estimate the Mn^{3+}/Mn^{4+} ratio. Low field AC susceptibility was measured using a home-made susceptometer [20]. $M(H)$ isotherms measured using a home-made vibrating sample magnetometer [21] were used for determining the magnetocaloric effect. DC resistivity measurements were done in the standard four-probe geometry.

XRD patterns for all the samples are shown in figure 2. All the diffractograms could be indexed to the orthorhombic *Pnma* space group. Table 1 summarizes the relevant structural parameters obtained by Rietveld analysis of the powder XRD data. As is seen from table 1, there is a systematic variation in the structural parameters. However, the maximum variation between the end members of the series is less than 1%, indicating that Al doping does not introduce any appreciable structural distortion. The *goodness* of the fits can be gauged by the ratio of R_{wp}/R_{exp}, which is around 1.15 for all the samples [22]. The values of the mean Mn valence determined using iodometry indicates that, on doping, Al predominantly replaces Mn^{4+} as was seen earlier in Al substituted $LaMnO_3$ [23]. This replacement of Mn^{4+} by Al^{3+} is evident from the monotonic decrease of B-site valence from 3.506 to 3.431. However, this makes the system non-stoichiometric and would result in the oxygen content varying from $3 + \delta$ to $3 - \delta$.

3. Results and discussions

3.1. AC susceptibility

The magnetic susceptibility is reported to drop in magnitude when cooled across the charge ordered transition in $Pr_{0.5}Ca_{0.5}MnO_3$ [10] showing a peak at the CO temperature. This

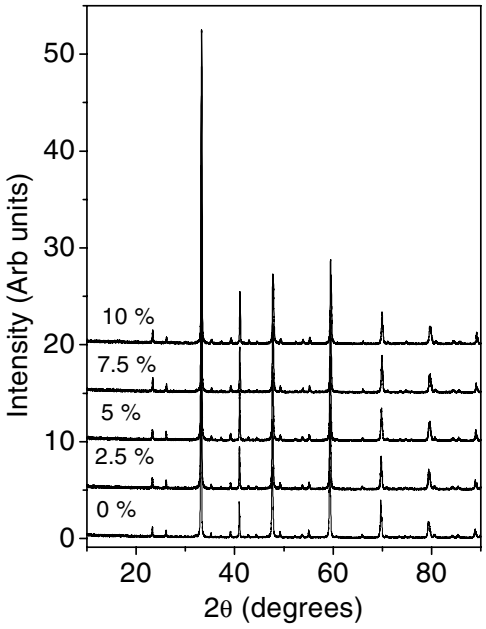

Figure 2. X-ray diffractograms for the series $Pr_{0.5}Ca_{0.5}Mn_{1-x}Al_xO_3$. All the samples crystallize in the orthorhombic phase, and the structural parameters derived from Rietveld profile refinement of the XRD data are given in table 1.

Table 1. Structural and fitting parameters determined from Rietveld profile refinement of the powder XRD patterns for the series $Pr_{0.5}Ca_{0.5}Mn_{1-x}Al_xO_3$. The mean valence state of Mn was determined by redox iodometric titrations.

Sample	$x = 0\%$	$x = 2.5\%$	$x = 5\%$	$x = 7.5\%$	$x = 10\%$
a (Å)	5.4057(2)	5.3993(2)	5.3948(2)	5.3894(4)	5.3836(3)
b (Å)	7.6138(3)	7.6101(2)	7.6055(3)	7.5962(2)	7.5912(2)
c (Å)	5.3954(2)	5.3920(2)	5.3892(2)	5.3859(4)	5.3836(3)
V (Å^3)	222.06	221.55	221.11	220.49	220.01
⟨Mn–O⟩ (Å)	1.942	1.943	1.939	1.936	1.932
⟨Mn–O–Mn⟩ (deg)	158.36	158.43	158.99	158.71	158.54
R_{wp}	19.35	18.82	18.58	18.82	18.64
R_{exp}	16.79	16.37	16.13	16.56	16.34
Mn^{3+} (%)	49.4	50.3	48.8	48.4	46.9
Mn^{4+} (%)	50.6	47.2	46.2	44.1	43.1

feature can be explained qualitatively to arise due to the structural transition (increasing orthorhombicity) driven by the ordering of the d_{z^2} orbitals of the Jahn–Teller distorted Mn^{3+} ion. When the system is cooled across the CO transition, the electrons get localized, consequently resulting in the FM spin fluctuations being replaced by AFM ones, giving rise to a rapid drop in the magnetic susceptibility. This has been experimentally observed through inelastic neutron scattering measurements on a similar charge and orbital ordered system $Bi_{1-x}Ca_xMnO_3$ [24]. The growth of the charge and orbital order promotes the magnetic phase transition at lower temperatures, and long range antiferromagnetism sets in at $T_N \approx 170$ K in the parent compound.

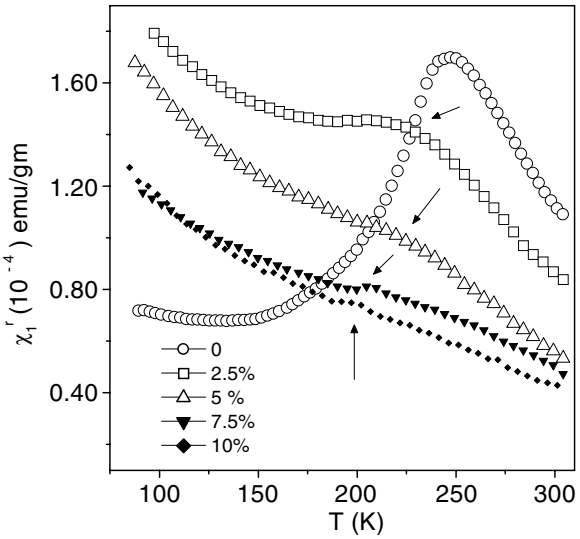

Figure 3. The real part of the first order AC susceptibility plotted as a function of temperature for the series $Pr_{0.5}Ca_{0.5}Mn_{1-x}Al_xO_3$. The arrows clearly show the suppression of the feature associated with charge ordering as a function of increasing Al doping.

Figure 3 shows the real part of the AC susceptibility (χ_1) measured for the series $Pr_{0.5}Ca_{0.5}Mn_{1-x}Al_xO_3$. The parent compound, $Pr_{0.5}Ca_{0.5}MnO_3$, is reported to undergo a charge ordering transition at $\approx$245 K, and as is seen in figure 3, the feature in susceptibility described above is clearly seen in the form of a peak in the first ordered susceptibility (χ_1). This feature is seen to decrease in magnitude and shift to lower temperatures with increasing Al doping, clearly indicating the weakening of the CO state. It is interesting to note that while previous reports have shown the CO state to be destroyed by small ($\sim$5% or less) amounts of impurity doping [15, 16], in our case traces of CO can be seen till up to 10% of Al doping. This is a reflection on both the robustness of the CO in the parent $Pr_{0.5}Ca_{0.5}MnO_3$ and the fact that Al does not introduce either lattice distortions or magnetic interactions of its own. Thus a gradual reduction in the CO strength is achieved using Al doping. *To the best of our knowledge this is the first observation of CO in a system with up to 10% of impurity doping at the Mn site*.

3.2. Magnetocaloric effect

The suppression of CO as seen in the low field AC susceptibility measurements was reconfirmed using the measurements of the magnetocaloric effect (MCE). MCE refers to the change in the isothermal magnetic entropy $|\Delta S_M|$ [25] produced by changes in the applied field, and is known to be appreciable in manganites across the CO transition, presumably due to the abrupt change in the magnetization coupled with a change in the lattice parameters [26, 27]. The CO transition being more first order like would involve a large change in magnetic entropy and would thus be expected to show up more prominently in MCE as compared to the AC susceptibility, which would be relatively insensitive to entropy changes. Moreover, it provides us with a quantitative estimate of the magnetic entropy change occurring at this transition. We have calculated $|\Delta S_M|$ through the measurement of classical $M(H)$ isotherms at different temperatures [28]. Each isotherm was measured after cooling the sample from 300 K, and adequate care was taken to ensure that the temperature stability was of the order of $\pm$0.005 K.

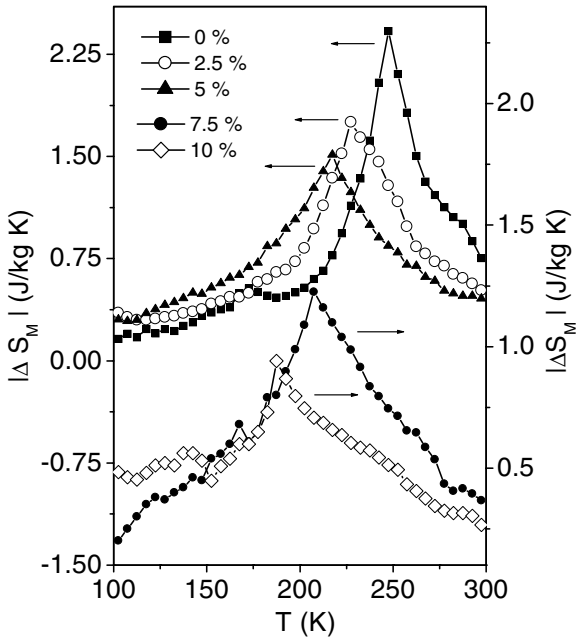

Figure 4. Temperature dependence of the magnetocaloric effect $|\Delta S_{\mathrm{M}}|$ for the series $Pr_{0.5}Ca_{0.5}Mn_{1-x}Al_xO_3$ at a field of 1 kOe. The peaks indicate the entropy change associated with the charge ordering, which is seen to decrease both in magnitude and in temperature with increasing Al doping.

The variation of the magnetic entropy and $M(H)$ isotherms are related by the thermodynamic Maxwell relation

$$\left(\frac{\partial S}{\partial H}\right)_T = \left(\frac{\partial M}{\partial T}\right)_H.$$

The isothermal entropy change can be calculated by means of magnetic measurements as

$$\Delta S_{\mathrm{M}}(T, H) = S_{\mathrm{M}}(T, H) - S_{\mathrm{M}}(T, 0) = \int_0^H \left(\frac{\partial M}{\partial T}\right)_{H'} \mathrm{d}H'.$$

For measurements made at discrete field and temperature values, it is given by

$$|\Delta S_{\mathrm{M}}| = \sum \frac{(M_n - M_{n+1})_H}{T_{n+1} - T_n} \Delta H_n$$

where M_n and M_{n+1} are the magnetization values measured at field H_n at temperatures T_n and T_{n+1} respectively. Figure 4 shows the temperature variation of $|\Delta S_{\mathrm{M}}|$ for the series $Pr_{0.5}Ca_{0.5}Mn_{1-x}Al_xO_3$. The magnitude of this magnetic entropy change associated with the CO transition is seen to reduce with Al doping, clearly indicating a gradual suppression of the CO strength with increasing Al substitution. It is to be noted that the temperatures of the peak in $|\Delta S_{\mathrm{M}}|$ match well with the temperatures where the feature in AC susceptibility is seen, and hence can be denoted as T_{CO}. Thus, the determination of the magnetocaloric effect unambiguously indicates that the feature observed in the susceptibility of the Al substituted samples corresponds to a weakened CO transition arising as a consequence of disorder introduced in the charge and orbitally ordered Mn network. In the parent $Pr_{0.5}Ca_{0.5}MnO_3$, a small peak in $|\Delta S_{\mathrm{M}}|$ at $T \approx 170$ K corresponding to the reported long range antiferromagnetic

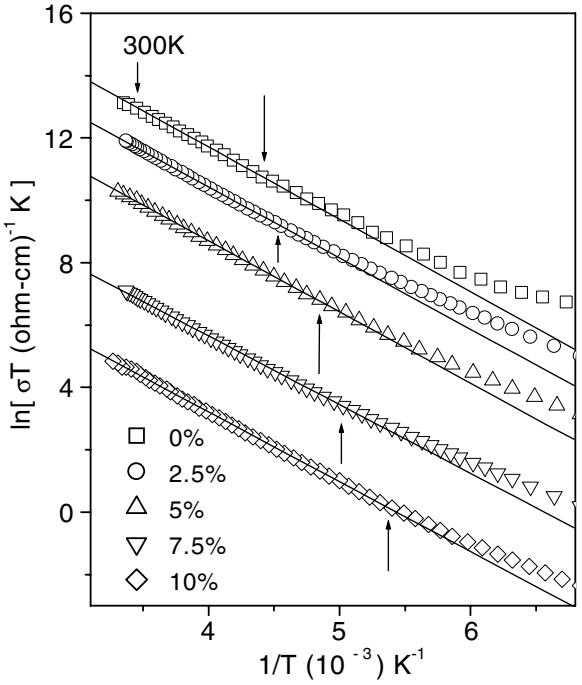

Figure 5. Semilog plot of σT versus $1/T$ for the series $Pr_{0.5}Ca_{0.5}Mn_{1-x}Al_xO_3$. The lines shows a linear fit to the conductivity data indicating adiabatic small polaronic hopping in the paramagnetic region. The arrows mark the temperature where the peak in the magnetocaloric effect corresponding to the CO transition is observed.

transition temperature (T_N) is observed. The doped samples do not show this feature in the measured temperature ranges due to the suppression of T_N with increasing substitution, the details of which are being published elsewhere [29].

3.3. Electron transport in the paramagnetic region

It is generally accepted [30] that the high temperature conductivity in manganites occurs through the hopping of charge carriers localized in the form of small polarons. These small polarons are known to form in systems with strong electron–phonon interactions, where the charge carriers are susceptible to self-localization through energetically favourable lattice distortions. In our case, this lattice distortion would be the Jahn–Teller distortion on the Mn^{3+} lattice site. If the lattice distortions are slow as compared to the charge carrier hopping frequencies, then the hopping is adiabatic and the conductivity can be written as

$$\sigma = ne\mu = \frac{3}{2}\frac{ne^2a^2\nu}{k_B}\frac{1}{T}\exp\left(\frac{-W_H}{k_BT}\right)$$

where n is the polaron density, e the electron charge, μ the polaron mobility, a the hopping distance, k_B the Boltzmann constant, ν the effective frequency at which the carrier tries to hop to a neighbouring site, and W_H the hopping energy. Thus, conductivity measurements fitted to a $\ln(\sigma T)$ versus $1/T$ plot should lead to a straight line. Figure 5 shows this fitting for the series $Pr_{0.5}Ca_{0.5}Mn_{1-x}Al_xO_3$. Good fits could be obtained for all the samples in the region $T > T_{CO}$, and the temperatures at which a deviation from the fit is seen match well with the

Table 2. Parameters determined from fitting the conductivity data on both sides of the CO transition for the series $Pr_{0.5}Ca_{0.5}Mn_{1-x}Al_xO_3$. The conductivity data for $T > T_{CO}$ are fitted to an adiabatic small polaron model, whereas the conductivity data in the region $T < T_{CO}$ are fitted to a 3D variable range hopping mechanism.

Sample	$x = 0\%$	$x = 2.5\%$	$x = 5\%$	$x = 7.5\%$	$x = 10\%$
W_H (meV)	185.7(9)	182.8(7)	180.7(8)	179.2(3)	176.2(3)
n (10^{21} cm^{-3})	2.225	2.270	2.207	2.195	2.132
T_0 (10^8 K)	7.593(8)	3.32(3)	3.13(6)	2.14(5)	2.07(9)

temperatures at which the feature associated with CO is seen in the magnetic measurements. It is interesting to note that conductivity in the paramagnetic region of the half-doped layered compound $LaSr_2Mn_2O_7$ has recently been ascribed to be due to the variable range hopping of polarons in the presence of a Coulomb gap [31]. However, our results differ, probably due to the difference in the nature of the samples used, and are seen to match well with data available on other 3D half-doped systems [32]. Table 2 summarizes the values determined from the fitting procedure. The activation energy for hopping is seen to reduce with Al doping. The change in the effective polaronic density is a reflection on the variation of the percentage of Mn^{3+} as a function of Al doping.

3.4. Electron transport in the CO region

The functional form of conduction in the charge ordered region is far more complicated, and remains to be understood. In systems with localized electron states, the variable range hopping (VRH) of polarons is a probable candidate for explaining the conduction process. This is possible if extrinsic effects like the presence of pinning centres create a non-zero density of states of charge excitations near the Fermi level, thus facilitating conduction through VRH. In general, the conductivity in 3D systems using Mott's VRH can be expressed as [33]

$$\sigma = \sigma_0 \exp(-T_0/T)^{1/4}$$

where T_0 is the Mott's activation energy (in units of K) and can be expressed as $T_0 \approx \frac{21}{k_B N(E)\xi^3}$, where k_B is Boltzmann's constant, $N(E)$ is the density of states, and ξ is the localization length. A semilog plot of σ versus $T^{-0.25}$ is shown in figure 6 for all the samples. The resistance (and the range of fit) is seen to decrease with increasing Al doping, indicating a destabilization of the insulating CO state. A decrease in the value of T_0 with doping (table 2) would imply an increase in the localization length (ξ), provided the density of states $N(E)$ does not change. Interestingly, charge ordered magnetite (Fe_3O_4) is also reported to show a similar VRH-like behaviour below the Verwey transition [34], indicating that VRH could be a generic feature in all systems with strong Coulombic interactions. The conductivity data when fitted to the variable range hopping model do not fit the whole temperature range below T_{CO}, indicating that there are other competing interactions at lower temperatures, which increase with increasing Al doping. A complete functional analysis would only be possible after considering other effects like phase separation, grain boundary scattering and Coulomb blockade effects.

4. Conclusions

In summary, polycrystalline samples of Al doped $Pr_{0.5}Ca_{0.5}MnO_3$ have been synthesized to study the effect of Mn site doping on CO. It is observed that Al preferentially replaces Mn^{4+} without introducing any appreciable change in structural parameters, and destabilizes the CO

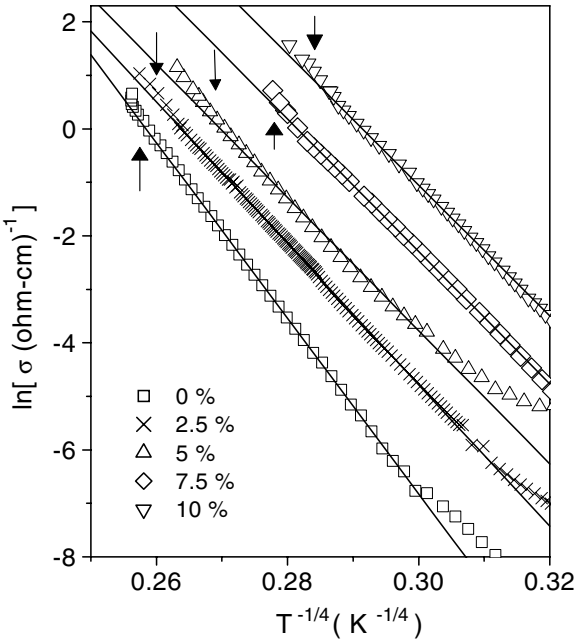

Figure 6. Semilog plot of σ versus $T^{-1/4}$ for the series $Pr_{0.5}Ca_{0.5}Mn_{1-x}Al_xO_3$. The lines are linear fits to the experimental data indicating that the variable range hopping mechanism is valid, at least in the temperature range close to the charge ordering transition.

state. However, traces of CO remain to up to 10% Al doping, as observed by measurements of AC susceptibility and the magnetocaloric effect. The conductivity in the paramagnetic region is seen to be through the adiabatic hopping of small polarons, which on cooling through the CO transition becomes of the VRH type at least near the CO transition. Since the collapse of the CO state at large applied magnetic fields is known to offer a promising avenue for achieving colossal magnetoresistance through the melting of charge ordering [35], it would be realistic to expect a substantial magnetoresistance in this series of samples at much lower applied fields through the melting of the weakened CO state.

Acknowledgments

We are grateful to Dr N P Lalla for help in x-ray diffraction and Mr Kranti Kumar for assistance in experimental work.

References

[1] Hardy V, Maignan A, Hebert S and Martin C 2003 *Phys. Rev.* B **67** 24401
[2] Maignan A, Hardy V, Martin C, Hebert S and Raveau B 2003 *J. Appl. Phys.* **93** 7361
[3] Raveau B, Hebert S, Maignan A, Fresard R, Hervieu M and Khomskii D 2001 *J. Appl. Phys.* **90** 1297
[4] Hebert S, Maignan A, Martin C and Raveau B 2002 *Solid State Commun.* **121** 229
[5] Katsufuji T, Cheong S W, Mori S and Chen C H 1999 *J. Phys. Soc. Japan* **68** 1090
[6] Li R-W, Sun J-R, Wang Z-H and Shen B-G 2000 *J. Appl. Phys.* **88** 5294
[7] Uehara M, Mori S, Chen C H and Cheong S W 1999 *Nature* **399** 560
[8] Radaelli P G, Ibberson R M, Argyriou D N, Casalta H, Andersen K H, Cheong S W and Mitchell J F 2001 *Phys. Rev.* B **63** 172419

[9] van den Brink J, Khaliullin G and Khomskii D 1999 *Phys. Rev. Lett.* **83** 5118
[10] Zirak J, Damay F, Hervieu M, Martin C, Raveau B, Andre G and Bouree F 2000 *Phys. Rev.* B **61** 1181
[11] Zimmermann M v, Hill J P, Gibbs D, Blume M, Casa D, Keimer B, Murakami Y, Tomioka Y and Tokura Y 1999 *Phys. Rev. Lett.* **83** 4872
[12] Zimmermann M v, Nelson C S, Hill J P, Gibbs D, Blume M, Casa D, Keimer B, Murakami Y, Kao C-C, Venkataraman C, Gog T, Tomioka Y and Tokura Y 2001 *Phys. Rev.* B **64** 195133
[13] Goodenough J B 1955 *Phys. Rev.* **100** 555
[14] Shannon R D and Prewitt C T 1969 *Acta Crystallogr.* B **25** 925
[15] Kimura T, Kumai R, Okimoto Y, Tomioka Y and Tokura Y 2000 *Phys. Rev.* B **62** 15021
[16] Levy P, Granja L, Indelicato E, Vega D, Polla G and Parisi F 2001 *J. Magn. Magn. Mater.* **226** 794
[17] Martin C, Magnan A, Damay F, Hervieu H, Raveau B, Jirak Z, Andre G and Bouree F 1999 *J. Magn. Magn. Mater.* **202** 11
[18] Damay F, Martin C, Maignan A and Raveau B 1998 *J. Magn. Magn. Mater.* **183** 143
[19] Young R A, Sakthivel A, Moss T S and Paiva-Santos C O 1994 *Users Guide to Program DBWS-9411* (Atlanta: Georgia Institute of Technology)
[20] Bajpai A and Banerjee A 1997 *Rev. Sci. Instrum.* **68** 4075
[21] Krishnan R V and Banerjee A 1999 *Rev. Sci. Instrum.* **70** 85
[22] Young R A (ed) 1993 *The Rietveld Method* (Oxford: Oxford University Press)
[23] Krishnan R V and Banerjee A 2000 *J. Phys.: Condens. Matter* **12** 3835
[24] Bao W, Axe J D, Chen C H and Cheong S-W 1997 *Phys. Rev. Lett.* **78** 543
[25] Tishin A M 1999 *Handbook of Magnetic Materials* vol 12, ed K H J Buschow (Amsterdam: Elsevier)
[26] Chen P, Du Y W and Ni G 2000 *Europhys. Lett.* **52** 589
[27] Sande P, Hueso L E, Miguens D R, Rivas J, Rivadulla F and Lopez-Quintela M A 2001 *Appl. Phys. Lett.* **79** 2040
[28] Foldeaki M, Chainine R and Bose T K 1995 *J. Appl. Phys.* **77** 3528
[29] Nair S and Banerjee A 2004 *Phys. Rev. Lett.* **93** 117204 (*Preprint* cond-mat 0401183)
[30] Salamon M B and Jaime M 2001 *Rev. Mod. Phys.* **73** 583
[31] Chen X J, Zhang C L, Gardner J S, Sarrao J L and Almasan C C 2003 *Phys. Rev.* B **68** 644051
[32] Quenneville E, Meunier M, Yelon A and Morin F 2001 *J. Appl. Phys.* **90** 1891
[33] Mott N F and Davies E A 1979 *Electronic Processes in Noncrystalline Solids* 2nd edn (Oxford: Clarendon)
[34] Gong G Q, Gupta A, Xiao G, Qian W and Dravid V P 1997 *Phys. Rev.* B **56** 5096
[35] Tomioka Y, Asamitsu A, Kawahara H, Moritomo Y and Tokura Y 1996 *Phys. Rev.* B **53** R1689